vector angle θ_0 is measured clockwise from the vertical. Figure 5.13(*b*) shows the regions of this initial condition space for which the particle exits through hole A (black) and for which it exits through hole B (blank). The dimension of the boundary separating these two regions is numerically found to be approximately 1.8. Blow-ups, however, reveal that there is the same sort of fine-scaled interweaving of fractal ($D_0 \approx 1.8$) and nonfractal ($D_0 = 1$) boundary regions as for the kicked double rotor example.

5.4 Chaotic scattering

In this section we consider the classical scattering problem for a conservative dynamical system.[4] The simplest example of this problem deals with the motion without friction of a point particle in a potential $V(\mathbf{x})$ for which $V(\mathbf{x})$ is zero, or else very small, outside of some finite region of space which we call the scattering region. Thus, the particle moves along a straight line (or an approximately straight line) sufficiently far outside the scattering region. We envision that a particle moves toward the scattering region from outside it, interacts with the scatterer, and then leaves the scattering region. The question to be addressed is how does the motion far from the scatterer after scattering depend on the motion far from the scatterer before scattering? As an example, consider Figure 5.14 which shows a scattering problem in two dimensions. The incident particle has a velocity parallel to the x-axis at a vertical displacement $y = b$. After interacting with the scatterer, the particle moves off to infinity with its velocity vector making an angle ϕ to the x-axis. We refer to the quantities b and ϕ as the impact parameter and the scattering angle, and we wish to investigate the character of the functional dependence of ϕ on b.

As an example consider the potential (Bleher *et al.*, 1990)

$$V(x, y) = x^2 y^2 \exp[-(x^2 + y^2)] \tag{5.6}$$

shown in Figure 5.15. This potential consists of four potential 'hills' with equal maxima at (x, y)-coordinate locations $(1, 1)$, $(1, -1)$, $(-1, 1)$, and $(-1, -1)$. The maximum value of the potential is $E_m = 1/e^2$. For large distances $r = (x^2 + y^2)^{1/2}$ from the origin, $V(x, y)$ approaches zero rapidly with increasing r. Figure 5.16(*a*) shows a plot of the *scattering function*, ϕ versus b, for the case where the incident particle energy E is larger than E_m. We observe for this case ($E/E_m = 1.626$) that the scattering function is a smooth curve. Furthermore, it is also found to be a smooth curve for all $E > E_m$. Figure 5.16(*b*) shows the scattering function for a case where $E < E_m$. We observe that the numerically computed dependence of ϕ on b is poorly resolved in the regions $0.6 \gtrsim \pm b \geq 0.2$. To

understand why this might be so, we note that Figure 5.16 is constructed by choosing a large number ($\sim 10^4$) of b-values evenly spaced along the interval of the b-axis shown in the plot. We then integrate the equation of motion for a particle of mass m, $m\mathrm{d}^2\mathbf{x}/\mathrm{d}t^2 = -\nabla V(\mathbf{x})$, for incident particles far from the potential for each b-value, and obtain the corresponding scattering angles ϕ. We then plot these angles to obtain the figure. Thus, the speckling of individually discernible points seen in Figure 5.16(b) in the region $0.6 \geq \pm b \geq 0.2$ might be taken to imply that the curve ϕ versus b varies too rapidly to be resolved on the scale determined by the spacing of b-values used to construct the figure. In this view one might still hope that sufficient resolution would reveal a smooth curve as in Figure 5.16(a). That this is not the case can be seen in Figures 5.17(a)–(c) which show successive magnifications of unresolved regions. Evidently magnification of a portion of unresolved region of Figure

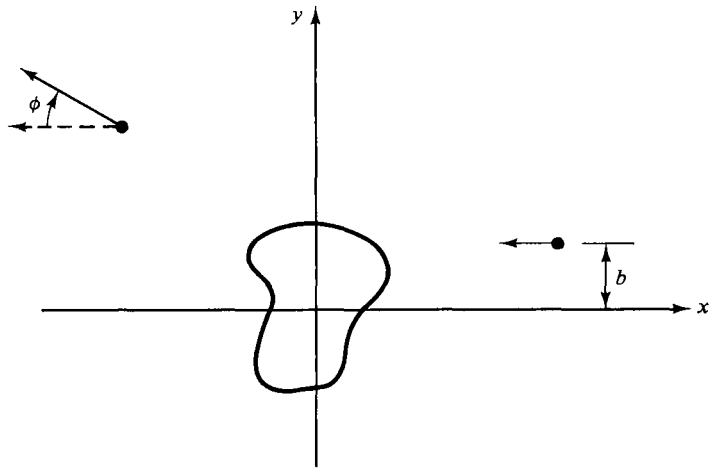

Figure 5.14 Scattering in two dimensions.

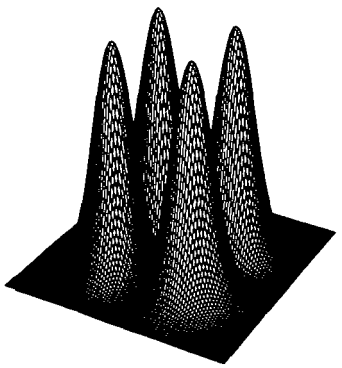

Figure 5.15 The potential $V(x, y) = x^2y^2\exp[-(x^2 + y^2)]$ (Bleher *et al.*, 1990).

5.16(*b*) by a factor of order 10^3 (Figure 5.17(*c*)) does not reveal a smooth curve. (This persists on still further magnification.) We call a value $b = b_s$ a singularity of the scattering function, if, for an interval $[b_s - (\Delta b/2), b_s + (\Delta b/2)]$, a plot of the scattering function made as in Figures 5.16 and 5.17 always shows unresolved regions for any interval length Δb, and, in particular, for *arbitrarily small* Δb. Another, more precise, way of defining b_s as a singularity of the scattering function is to say that, in any small interval $[b_s - (\Delta b/2), b_s + (\Delta b/2)]$, there is a pair of b-values which yields scattering angles whose difference exceeds some value $K > 0$ which is ***independent*** of Δb. (That is arbitrarily small differences in b yield ϕ-values which differ by order 1.) The interesting result concerning the scattering function shown in Figure 5.16(*b*) is that the set of singular b-values is a fractal. Bleher *et al.* (1990) calculate a fractal dimension of approximately 0.67 for the singular set. We call the phenomenon seen in Figure 5.16(*b*) *chaotic scattering* as distinguished from the case of ***regular scattering*** (Figure 5.16(*a*)). (The transition from regular to chaotic scattering as the energy is lowered from the value in Figure 5.16(*a*) to the value in Figure 5.16(*b*) will be discussed in Chapter 8.)

The chaotic scattering phenomenology we have described above is a

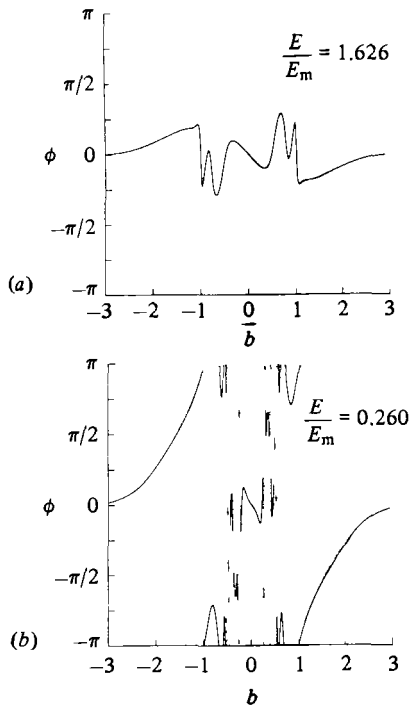

Figure 5.16 Scattering functions ϕ versus b for (*a*) $E/E_m = 1.626$ and (*b*) $E/E_m = 0.260$ (Bleher *et al.*, 1990).

general feature of a large class of problems. Chaotic scattering has appeared in numerous applications including celestial mechanics (Petit and Hénon, 1986), the scattering of vortices in fluids (Eckhardt and Aref, 1988), scattering of microwaves (Doron *et al.*, 1990), the conversion of magnetic field energy to heat in solar plasmas (Lau and Finn, 1991). chemical reactions (Noid *et al.*, 1986), collisions between nuclei (Rapisarda and Baldo, 1991), and conductance fluctuations in very tiny two-dimensional conductor junctions (Jalabert *et al.*, 1990). The latter three examples are cases where it becomes important to consider the

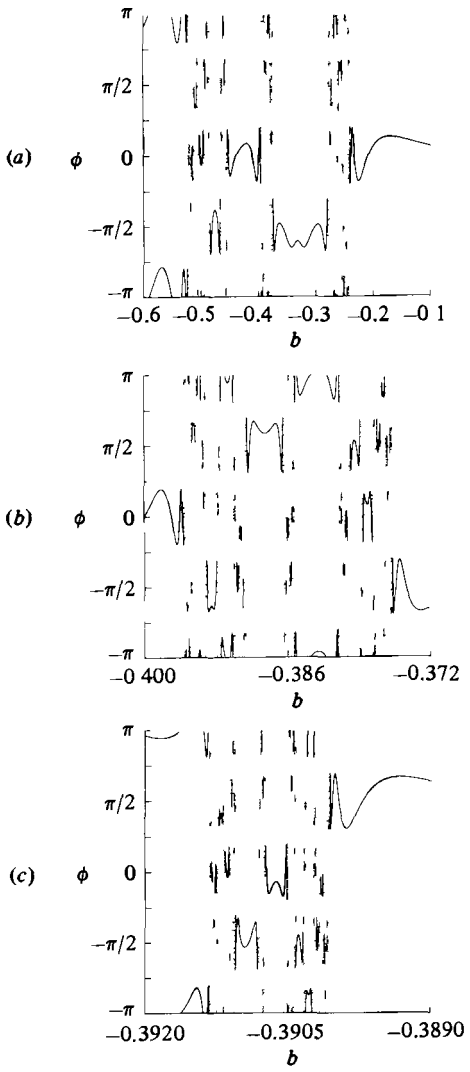

Figure 5.17 Successive magnifications of the scattering function (*a*) for a small *b* interval in Figure 5 16(*b*), (*b*) for a small *b* interval in Figure 5 17(*a*), and (*c*) for a small *b* interval in Figure 5 17(*b*) (Bleher *et al*, 1990)

quantum mechanical treatment of a problem whose classical counterpart exhibits chaotic scattering. For further material on the quantum aspects of chaotic scattering see Blümel (1991), Cvitanović and Eckhardt (1989), Gaspard and Rice (1989a,b,c), and Blümel and Smilansky (1988).

5.5 The dynamics of chaotic scattering

How does the dynamics of the scattering problem lead to the phenomena we have observed in Figures 5.16(*b*) and 5.17? In order to gain some insight into this question we plot in Figure 5.18 the 'time delay' (the amount of time that a particle spends in the scattering region bouncing between the hills) as a function of the impact parameter b for the potential (5.6) with the same particle energy as for Figures 5.16(*b*) and 5.17. We see that the regions of poor resolution of the scattering function (cf. Figures 5.16(*b*) and 5.17) coincide with b-values for which the time delay is long. Indeed careful examination of magnifications suggests that the singularities of the scattering function coincide with the values of b where the time delay is infinite. Very near a value of b for which the time delay is infinite the time delay will be very long, indicating that the incident particle

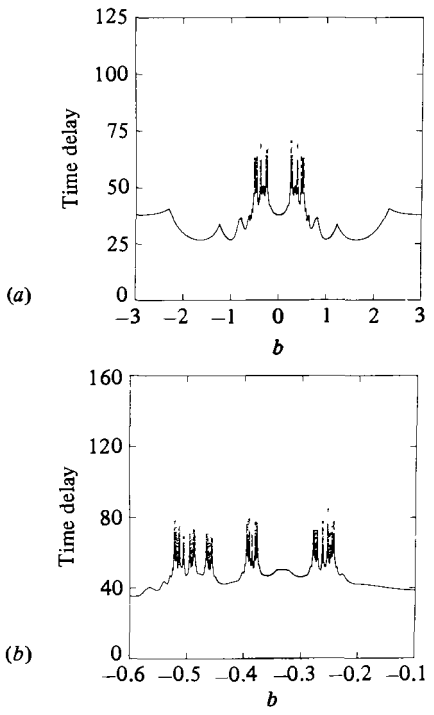

Figure 5.18 Time delay versus impact parameter for the b intervals (*a*) corresponding to that in Figure 5.16(*b*), and (*b*) corresponding to that in Figure 5.17(*a*) ($E/E_m = 0.260$) (Bleher *et al.*, 1990).

experiences many bounces between potential hills before leaving the scattering region. Say we choose a b-value yielding a long time delay for which the particle experiences say 1000 bounces before exiting the scattering region. Now change b very slightly so as to increase the delay time by a small percentage yielding say 1001 bounces before the particle exits the scattering region. The presence of this one extra bounce means that the scattering angle for the two cases can be completely different. Hence, we expect arbitrarily rapid variations of ϕ with b near a b-value yielding an infinite time delay, and we may thus conclude that these values coincide with the singularities of the scattering function. The effect is illustrated in Figure 5.19 which shows two orbit trajectories whose b values differ by 10^{-8}. The orbit in Figure 5.19(a) ($b = -0.39013269$) experiences about 14 bounces (depending on how you define a bounce). The orbit in Figure 5.19(b) ($b = -0.39013268$) is very close to that in Figure 5.19(a) for the first 13 or so bounces but subsequently experiences about 4 more bounces than the orbit in Figure 5.19(a). The two orbits have completely different scattering angles, one yielding scattering upward (Figure 5.19(a)) and the other yielding scattering downward.

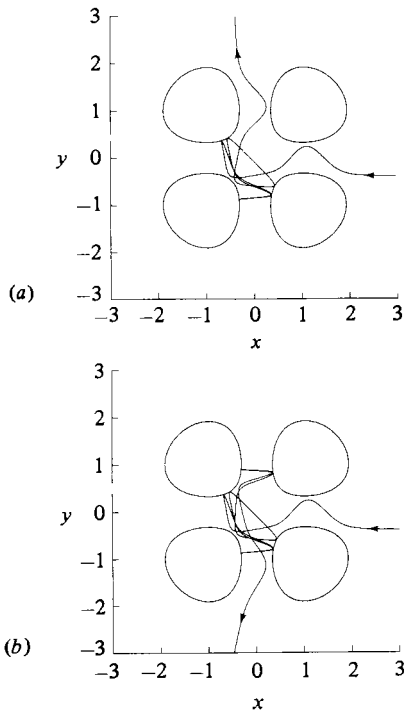

Figure 5.19 Orbits for particles with slightly different impact parameters (differing by 10^{-8}): (a) $b = -0.39013269$, and (b) $b = -0.39013268$. The four closed solid curves are the contours $V(x, y) = E = 0.260E_m$ (Bleher *et al.*, 1990).

The interpretation of these results is as follows. The equations of motion are four-dimensional,

$$m\,\mathrm{d}\mathbf{v}/\mathrm{d}t = -\nabla V(\mathbf{x}), \tag{5.7a}$$

$$\mathrm{d}\mathbf{x}/\mathrm{d}t = \mathbf{v}, \tag{5.7b}$$

where $\mathbf{x} = (x, y)$ and $\mathbf{v} = (v_x, v_y)$, but because the particle energy,

$$E = \tfrac{1}{2}m\mathbf{v}^2 + V(\mathbf{x}), \tag{5.8}$$

is conserved, we may regard the phase space as being three-dimensional. (For example, we can regard the phase space as consisting of the three variables, x, y, θ, where θ is the angle the vector $\mathbf{v}$ makes with the positive x-axis. These three variables uniquely determine the system state, x, y, v_x, v_y, because (5.8) gives $|\mathbf{v}|$ in terms of x and y, $|\mathbf{v}| = [2(E - V(\mathbf{x}))/m]^{1/2}$.) The presence of infinite time delays on a fractal set of b-values is due to the existence of a nonattracting chaotic invariant set that is in a bounded region of phase space. Orbits on this invariant set bounce forever between the hills never leaving the scattering region both for $t \to +\infty$ and for $t \to -\infty$. This chaotic set is essentially the intersection of its stable and unstable manifolds, each of which locally consists of a Cantor set of approximately parallel two-dimensional surfaces in the three-dimensional phase space. Thus, the stable and unstable manifolds are each fractal sets of dimension between 2 and 3.

We have, in numerically obtaining our scattering function plots, taken initial conditions at some large x-value $x = x_0$ and have chosen the initial angle θ_0 between $\mathbf{v}$ and the positive x-axis to be $\theta_0 = \pi$ (i.e., $v_{y_0} = 0$ and $v_{x0} < 0$; see Figure 5.14). This defines a line in the space (x, y, θ) which we regard as the phase space. This line of initial conditions generically intersects the stable manifold of the nonattracting chaotic invariant set in a Cantor set of dimension between zero and one[2] (cf. Eq. (3.46)). It is this intersection set that is the set of singular b-values of the scattering function. Since these b-values correspond to initial conditions on the stable manifold of the chaotic invariant set, the orbits they generate approach the invariant set as $t \to +\infty$; hence they never leave the scattering region.

Figure 5.20(*a*) shows a numerical plot of the $y = 0$ cross section of the stable manifold of the chaotic invariant set. This plot is created by taking a grid of initial conditions in (x_0, θ_0) and integrating them forward in time. Then only those initial conditions yielding long delay times are plotted. We observe that the stable manifold intersection appears as smooth (and swirling) along one dimension with (poorly resolved) fine-scale (presumably fractal) structure transverse to that direction. Figure 5.20(*b*) shows a similar plot of the intersection of the unstable manifold with the $y = 0$ plane obtained by integrating initial conditions on the grid backwards in

time and again plotting those initial conditions whose orbits remain in the scattering region for a long time. We see that the unstable manifold picture is a mirror image (through the line $x_0 = 0$) of the stable manifold picture. This is a result of the time reversal symmetry[5] of Eqs. (5.7) (they are invariant to the transformation $\mathbf{v} \to -\mathbf{v}, t \to -t$) and the symmetry of the potential (5.6). In particular this means that the stable and unstable manifolds have the same fractal dimension. Figure 5.20(*c*) shows the

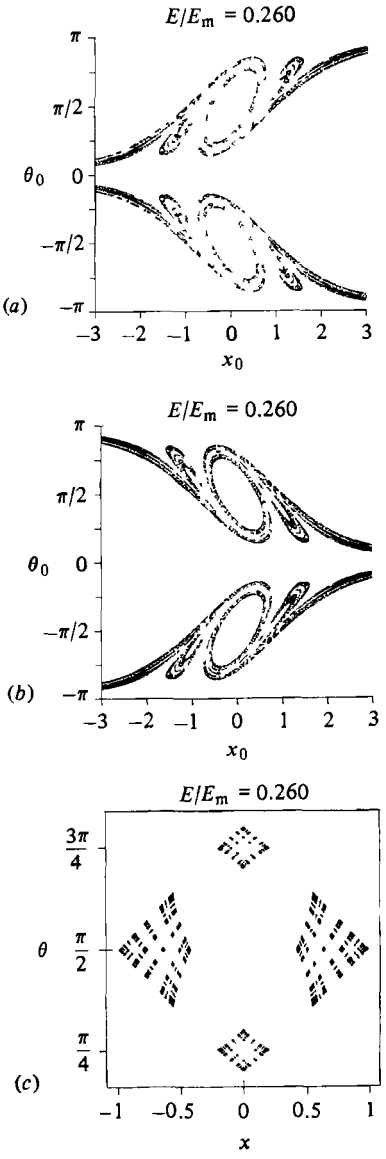

Figure 5.20 Intersection with the $y = 0$ surface of section of (*a*) the stable manifold, (*b*) the unstable manifold, and (*c*) the nonattracting chaotic invariant set (Bleher *et al.*, 1990).

intersection of the chaotic invariant set with the plane $y = 0$. This picture is consistent with the invariant set being the intersection of its computed stable and unstable manifolds (i.e., the set shown in Figure 5.20(*c*) is the intersection of the sets shown in Figures 5.20(*a*) and (*b*)). Apparently, these intersections occur with angles bounded well away from zero. Hence, there appear to be no tangencies between the stable and unstable manifolds, thus supporting the idea that, in this case, the dynamics on the invariant set is hyperbolic. (See Bleher *et al.* (1990) for a description of how Figure 5.20(*c*) is numerically computed. This computation makes use of a numerical technique for obtaining unstable chaotic sets which is discussed and analyzed by Nusse and Yorke (1989); see also Hsu *et al* (1988).)

The existence of a Cantor set of singular b-values for the scattering function implies that it will often be very difficult to obtain accurate values of the scattering angle if there are small random experimental errors in the specification of b. This situation is similar to that which exists when there are fractal basin boundaries.[6] Indeed we can employ a modification of the uncertainty exponent technique of Section 5.2 to obtain the fractal dimension of the singular set. We observe that, for our example (Eq. (5.6) with $E/E_m = 0.260$), small perturbations about a singular b-value can lead to either upward scattering ($0 \leq \phi \leq \pi$ as in Figure 5.19(*a*)) or downward scattering ($-\pi \leq \phi \leq 0$ as in Figure 5.19(*b*)). Thus, we randomly choose many values of b in an interval containing the Cantor set. We then perturb each value by an amount ε and determine whether the scattering is upward or downward for each of the three impact parameter values, $b - \varepsilon$, b and $b + \varepsilon$. If all three scatter upward or all three scatter downward, we say that the b-value is ε-certain, and, if not, we say it is ε-uncertain. We do this for several ε-values and plot on a log–log scale the fraction of uncertain b-values $\bar{f}(\varepsilon)$. The result is shown in Figure 5.21 which shows a good straight line fit to the data indicating a power law dependence $\bar{f}(\varepsilon) \sim \varepsilon^{\alpha}$. The exponent α is related to the dimension of the set of singular b-values by

$$D_0 = 1 - \alpha \tag{5.9}$$

(i.e., Eq. (5.3b) with $N = 1$ corresponding to the fact that the initial conditions of the scattering function lie along a line in the three-dimensional phase space). The straight line fit in Figure 5.21 yields a slope of $\alpha = 0.33$ corresponding to a fractal dimension of $D_0 = 0.67$ for the scattering function of Figure 5.16(*b*) and 5.17. The dimension of the stable and unstable manifolds in the full three-dimensional phase space is $2 + D_0$, and the dimension of their intersection (which is the dimension D_{cs} of the chaotic set) is (cf. Eq. (3.46))

$$D_{cs} = 2D_0 + 1. \tag{5.10}$$

The dimension of the intersection of the chaotic set with the $y = 0$ plane[2] (i.e., the dimension of the set plotted in Figure 5.20(*c*)) is $2D_0$.

In all of our discussion of chaotic scattering we have been concerned with a particular illustrative example of scattering in two degrees of freedom (i.e., the two spatial dimensions x and y). The phenomena we see are typical for two-degree-of-freedom scattering. Other works on chaotic scattering have also tended to be for examples with two degrees of freedom. The possibility of new chaotic scattering phenomena in systems with more than two degrees of freedom remains largely unexplored. An exception is the paper of Chen *et al.* (1990b) who consider the question of whether the presence of a chaotic invariant set in the phase space implies a fractal set of singularities in a scattering function plot (i.e., a plot giving an after-scattering variable as a function of a single before-scattering variable). They find that, when the number of degrees of freedom is greater than 2, the scattering function typically does not exhibit fractal behavior, even when the invariant set is fractal and chaotic, unless the fractal dimension of the invariant set is large enough,

$$D_{cs} > 2M - 3, \tag{5.11}$$

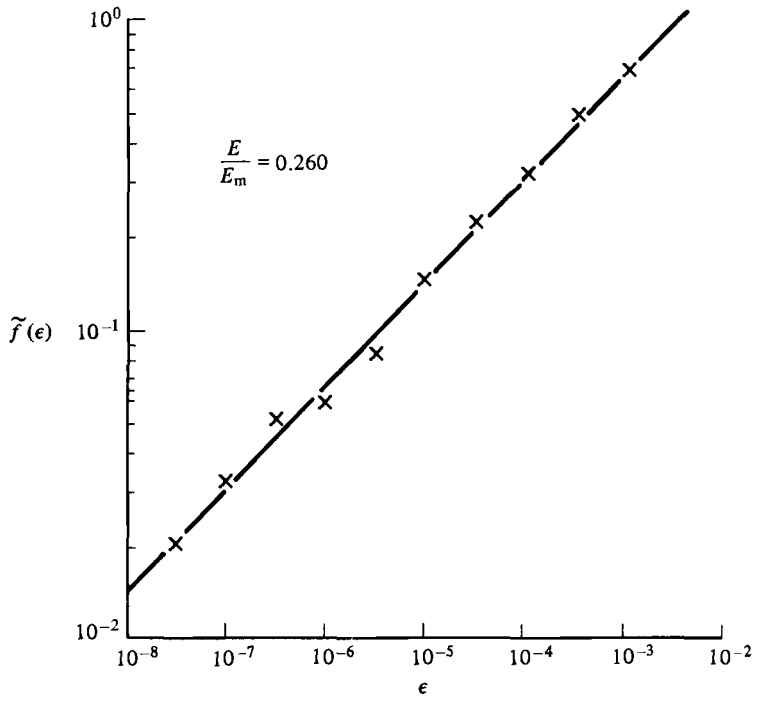

Figure 5.21 $\tilde{f}(\varepsilon)$ versus ε for the scattering function in the interval shown in Figure 5.17(*b*). The slope yields a fractal dimension of approximately 0.67 ($E/E_m = 0.260$) (*Bleher et al.*, 1990).

where M is the number of degrees of freedom.[7] Since D_{cs} for $M = 2$ is greater than 1 in the fractal case, we see that Eq. (5.11) is always satisfied in chaotic two-degree-of-freedom potential scattering problems. In the case of three-degree-of-freedom systems, however, we require $D_{cs} > 3$. Chen *et al.* illustrate this numerically for the simple three-dimensional scattering system consisting of four hard reflecting spheres of equal radii with centers located on the vertices of a regular tetrahedron, as illustrated in Figure 5.22. They show numerically that as the sphere radius increases, D_{cs} increases from below 3 to above 3, and this is accompanied by the appearance of fractal behavior in typical scattering functions.

5.6 The dimensions of nonattracting chaotic sets and their stable and unstable manifolds

We have seen in Chapter 4 that there is an apparent relationship between the Lyapunov exponents of a chaotic attractor and its information dimension (Eqs. (4.36)–(4.38)). In this section we will show that the same is true for nonattracting chaotic invariant sets of the type that arise in chaotic transients, fractal basin boundaries, and chaotic scattering (Kantz and Grassberger, 1985; Bohr and Rand, 1987; Hsu *et al.*, 1988). In particular, we treat the case of a smooth two-dimensional map $\mathbf{M}(\mathbf{x})$ which has a nonattracting variant chaotic set Λ. In Figure 5.23 we schematically picture the invariant set as being the intersection of stable and unstable manifolds. Let B, also shown in the figure, be a compact set containing the invariant set such that under the action of $\mathbf{M}$ almost all points (with respect to Lebesgue measure) eventually leave B and never return. The only initial conditions that generate forward orbits which remain forever in B are those which lie on the invariant set and its stable manifold. Thus, part of B must map out of B and the Lebesgue measure (area) which remains in B is decaying.

Say, we randomly sprinkle $N(0)$ points uniformly in B. After iterating these points for t iterates, only $N(t) < N(0)$ have not yet left. The average

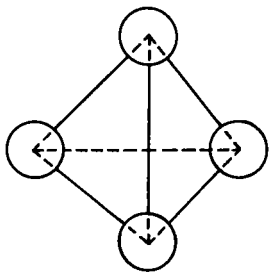

Figure 5.22 Scatterer consisting of four equal radii hard spheres with centers located on the vertices of a regular tetrahedron.